



Green Synthesis of Nanochitosan/Bentonite/ SnO_2 -ZnO Bionanocomposite for Removal of Heavy Metal Ions and Photocatalytic Degradation of Organic Dye

Somayeh Heydari¹ · Mehdi Moradi²

Accepted: 30 December 2023 / Published online: 8 February 2024

© The Author(s), under exclusive licence to Springer Science+Business Media, LLC, part of Springer Nature 2024

Abstract

Biotreatment of wastewater has attracted considerable attention due to its low cost and eco-friendliness. This study developed a novel bionanocomposite comprised of Nanochitosan (NCS), Bentonite (Bt), and SnO_2 -ZnO nanocomposite prepared using *Salvia officinalis* extract as a reducing/stabilizing agent. The NCS/Bt/ SnO_2 -ZnO bionanocomposite exhibited a rough surface with porous nature. EDX, XRD, and FTIR results confirmed the formation of the bionanocomposite. TGA indicated high thermal stability of the NCS/Bt/ SnO_2 -ZnO. DRS results revealed that the bionanocomposite had a band gap of 2.60 eV. The surface area of NCS/Bt/ SnO_2 -ZnO was found to be $32.54 \text{ m}^2 \text{ g}^{-1}$ with a 17.98 nm pore size. Adsorption of Fe(III) and Pb(II) ions and photocatalytic degradation of methylene blue (MB) dye using this bionanocomposite were studied. Under optimal conditions, the highest removal of Fe(III) (99.5%) and Pb(II) (91.5%) was achieved after 5 min and 40 min, respectively. The adsorption data fitted the Langmuir isotherm and indicated the removal capacity of 555.55 and 243.90 mg g^{-1} for Fe(III) and Pb(II), respectively. Also, the NCS/Bt/ SnO_2 -ZnO showed the MB dye degradation efficiency of 99% within 30 min. Therefore, the NCS/Bt/ SnO_2 -ZnO can be used as an environmentally friendly, cost-effective, thermally stable, and high-performance adsorbent/photocatalyst to remove heavy metal ions and dye molecules.

Keywords Green synthesis · Nanochitosan/Bentonite/ SnO_2 -ZnO · Heavy metal adsorption · Photocatalytic activity

Introduction

Environmental water pollution due to heavy metal ions and toxic dyes seriously threatens the human life and ecosystems. These pollutants have originated from mining activities, metal coating, dye manufacturing, leather tanning, textile, tannery, papermaking, pesticides, printing, plastics, photographic industries, petroleum refining, and food technology [1]. The existence of heavy metals and toxic dyes in water systems has posed a severe threat to the environment owing to their toxicity, non-biodegradability, carcinogenic, and mutagenic potential [2–4]. Thus, the development of simple, environmentally friendly, and cost-effective methods

to remove these hazardous pollutants from wastewater systems has become a crucial issue.

Recently, bionanocomposites have attracted significant attention for water and wastewater treatment because of their biocompatibility, eco-friendly, nontoxicity, abundance, low-cost, biodegradation, and ease of preparation [5, 6]. These hybrid materials are composed of biopolymers and inorganic solids with at least one dimension in the nanometric range. The addition of nanoscale inorganic fillers to biopolymer results in the synthesis of novel materials with superior mechanical, thermal, and chemical characteristics. The modification of biopolymer increases the surface area with a large number of reaction sites for effective removal of pollutants. Chitosan (CS), a polysaccharide composed mainly of units of D-glucosamine and N-acetyl-D-glucosamine, is one of the most abundant natural biopolymers. This copolymer is a very promising candidate for wastewater treatment because of the presence of high content of functional groups (OH and NH_2) in its structure, serving as coordination and reaction sites [7]. The recent widespread application of chitosan

✉ Somayeh Heydari
s.heydari@tjamcaas.ac.ir

¹ Department of Chemistry, University of Torbat-e Jam, Torbat-e Jam, Iran

² Department of Horticultural Science, University of Torbat-e Jam, Torbat-e Jam, Iran

has attracted considerable attention for synthesizing its derivatives at the nanoscale. The nanochitosan (NCS) is a non-toxic and stable polyanion that exhibits excellent physicochemical properties [8, 9]. The large surface area, compactness, and high mechanical strength increase the applications of NCS in water treatment compared to chitosan. Therefore, in this work, NCS was used as a precursor to develop a bionanocomposite.

Recent studies show that modifying biopolymer with the nanofiller clay minerals reinforces its properties [10, 11]. The widespread application of clays is due to their economic and environmental advantages. Bentonite (Bt) is a layered aluminosilicate clay consisting mainly of montmorillonite. It has a high absorption ability and exhibits good thermal and mechanical stability. The Bt, as an environmentally friendly and cost-effective nanofiller in the bionanocomposite, not only improves its mechanical strength but also provides a high specific surface area and abundance of active sites for pollutant remediation [12].

The functional properties of bionanocomposites can be improved by incorporating metal oxide nanoparticles [13]. Owing to their high surface-volume ratio and highly reactive sites, metal oxide nanoparticles have attracted significant attention in widespread practical applications such as wastewater treatment, food packaging, drug delivery, and biosensors [14–17]. For instance, ZnO and SnO₂ nanoparticles have been extensively used due to their environmental friendliness, low cost, high activity, simplicity of preparation, and long-term stability [6, 18]. The unique properties of these nanoparticles make them promising candidates for use in commercial products and industrial processes, including water remediation. The simultaneous use of these two nanoparticles is an effective strategy to enhance the performance of nanocomposite. SnO₂–ZnO nanocomposite, with its eco-friendly nature and outstanding optical and mechanical properties, has demonstrated high efficiency in wastewater treatment [19, 20].

In recent years, the photosynthesis of metal oxide nanoparticles by plants as one of the synthesis pathways has attracted considerable attention [21]. Active ingredients such as Tannins, polyphenols, flavonoids, amino acids, inorganic ions, sugars, alkaloids, and organic acids present in the plant extracts support the formation of nanomaterials. These primary and secondary metabolites can play a natural reducing and stabilizing role in the production of nanoparticles. Various plants, including *Arachis hypogaea*, *Phlomis cancellata* Bunge, *Bridelia retusa*, *Tinospora cordifolia*, *Cocoa*, *Muntingia calabura*, and *Tabebuia aurea* have been utilized to synthesize nanoparticles [22–29]. Green synthesis of nanoparticles using plant extracts is facile, rapid, economical, and requires no elevated reaction conditions, and toxic chemicals. Furthermore, the fabricated nanomaterials are non-toxic, stable, and biologically compatible.

Salvia officinalis is a medicinal plant belonging to the Labiate family. This plant grows mainly in the Mediterranean and Middle East regions, but it is today found worldwide. *Salvia officinalis* is a valuable source of phenolic acids and flavonoids, which may be responsible for the formation of metal nanoparticles [30].

In the current work, for the first time, we developed a facile and green approach for the preparation of Nanochitosan/Bentonite/SnO₂–ZnO (NCS/Bt/SnO₂–ZnO) bionanocomposite using low-cost and environmentally friendly materials. For this purpose, SnO₂–ZnO nanocomposite was prepared in the presence of *Salvia officinalis* aqueous extract as the reducing agent under mild conditions. Then, bionanocomposites based on NCS incorporated with these eco-friendly SnO₂–ZnO nanocomposites and Bt were synthesized, and their properties were investigated. Modifying NCS with SnO₂–ZnO nanocomposites and Bt provided better thermal stability, high specific surface area, and abundant reactive sites. NCS/Bt/SnO₂–ZnO bionanocomposite was applied for the adsorptive removal of heavy metal ions of Fe(III) and Pb(II) and photodegradation of methylene blue (MB) dye from water.

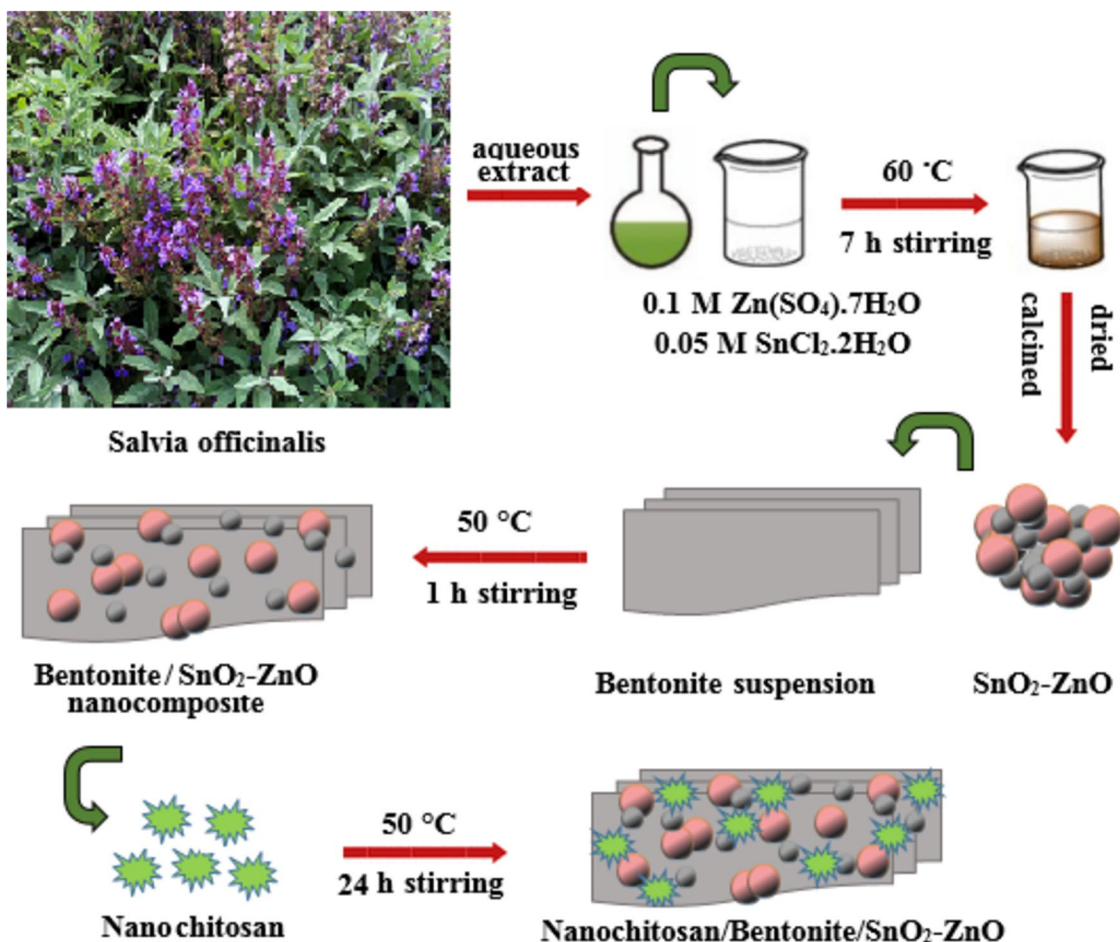
Experimental

Materials

Chitosan, Sodium tripolyphosphate (TPP), Zn (SO₄)_{0.7}H₂O, and SnCl₂·2H₂O were obtained from Sigma Aldrich. Bt was purchased from Zarin Khak Ghayen company, Iran. Standard solutions of Fe(III) or Pb(II) (1000 mg L⁻¹) were of analytical grade and purchased from Chem-Lab nv. MB dye (MW = 374.2, λ_{max} = 665 nm) was provided by Merck and employed without further purification.

Nanochitosan Preparation

NCS was prepared from the chitosan by ionotropic gelation method with tripolyphosphate (TPP) ions [31]. Initially, to obtain the transparent homogeneous solution of chitosan, 1.0 g of chitosan was added into 100 mL of acetic acid solution (2% v/v) and stirred for 30 min. Subsequently, 0.8 g of TPP dissolved in deionized water was added dropwise under continuous stirring for 2 h. The resulting milky emulsion was centrifuged for 20 min at 16,000 rpm, and the NCS formed was rinsed with double distilled water three times. Finally, the nanoparticles were air-dried at ambient temperature for 48 h.



Scheme 1 Schematic diagram for the synthesis of the NCS/Bt/SnO₂/ZnO bionanocomposite

Salvia Officinalis Extract Preparation

Salvia officinalis leaves were washed with deionized water to remove dirt and kept to dry at ambient temperature. To prepare plant extract, 10 g of powders was added to 100 mL deionized water and stirred for 2 h at 70 °C. Then, the suspension was cooled at room temperature, and filtered by Whatman No 1 filter paper. The obtained solution was stored in a refrigerator to synthesize SnO₂/ZnO nanocomposite.

Biosynthesis of the SnO₂/ZnO Nanocomposite

To synthesize SnO₂/ZnO nanocomposite, 25 mL of 0.1 M Zn(SO₄)0.7H₂O was mixed with 25 mL of 0.05 M SnCl₂ 2H₂O and stirred at ambient temperature for 30 min. 200 ml of the Salvia officinalis aqueous extract was then added dropwise to this stirring solution during 30 min, and subjected for 7 h stirring at 60 °C. The resulting suspension was centrifuged, filtered, washed with distilled water, and dried in the oven for 2 h at 50 °C. Finally, the obtained ZnO/SnO₂ nanocomposites were calcined at 600 °C for 2 h.

Preparation of Nanochitosan/Bentonite/SnO₂-ZnO Biocomposite

Initially, a suspension of Bt was obtained by dispersing 1 g of Bt in 100 mL of distilled water with stirring for 12 h. Subsequently, 0.3 g of SnO₂/ZnO aqueous suspension was added dropwise to the Bt suspension under stirring for 1 h at 50 °C. The resulting mixture was slowly added to the solution of NCS (1% w/v) in acetic acid (1% v/v) and stirred for 24 h at 50 °C. The as-prepared NCS/Bt/SnO₂-ZnO bionanocomposite was subsequently filtered, washed, and dried at ambient temperature for three days. A schematic representation for the synthesis of NCS/Bt/SnO₂-ZnO bionanocomposite is shown in Scheme 1.

Characterization Techniques

The surface morphologies of the synthesized materials were characterized by employing a TESCAN, MIRA3 field emission scanning electron microscopy (FESEM) coupled with an energy dispersive analyzer (EDX). X-ray

diffraction (XRD) study was performed to determine the crystalline phases of the samples on a Philips X-ray diffractometer, Siemens D-5000 (Germany). The FTIR spectra of the materials were taken using AVATAR 370 FTIR spectrometer (USA) at the range of 400–4000 cm^{-1} . The thermal properties of the synthesized samples were analyzed by thermogravimetric analysis (TGA) on an SDT Q600 V20.9 Build 20 apparatus under an air atmosphere in the temperature range of 25–900 $^{\circ}\text{C}$. The differential scanning calorimetry (DSC) studies were performed with a DSC Q600 instrument (USA) under an air atmosphere. The UV–vis diffuse reflectance spectra (DRS) were monitored on Scinco, S-4100 spectrophotometer (South Korea). The Brunauer–Emmett–Teller (BET) surface area and pore size measurements of the materials were performed using BELSORP mini-II (Japan) via the low-temperature N_2 adsorption method.

Adsorption Studies

The adsorption experiments were carried out by batch methods in glass flasks containing the as-prepared materials and 10 mL (50 mg L^{-1}) of Fe(III) and Pb(II) aqueous solutions at room temperature. Initial pH values were adjusted by adding 1 $\text{mol}\cdot\text{L}^{-1}$ solutions of NaOH or HCl. Then, the mixtures were shaken with a constant stirring speed of 160 rpm under a dark environment. After a specific time interval, the adsorbents were collected, and the amount of remaining concentrations of target ions was determined by atomic absorption technique. Effects of adsorption time, initial heavy metal concentration, adsorbent dose, and initial pH, on the extent of removal were studied.

The adsorption kinetics of Fe(II) and Pb(II) on the as-synthesized nanocomposites were assessed using pseudo-first-order [Eq. (1)], and pseudo-second-order [Eq. (2)] models [32].

$$\log (q_e - q_t) = \log q_e - k_1 t / 2.303 \quad (1)$$

$$t/q_t = 1/k_2 q_e^2 + t/q_e \quad (2)$$

Here, q_e and q_t are the amount of metal ion adsorbed (mg g^{-1}) at equilibrium time and at time t (min), respectively. The k_1 (min^{-1}) is the first-order rate constant, and k_2 ($\text{g mg}^{-1} \text{min}^{-1}$) is the second-order rate constant.

To evaluate the adsorption mechanism of Fe(III), and Pb(II) ions by the NCS/Bt/SnO₂-ZnO bionanocomposite, Langmuir [Eq. (3)], and Freundlich [Eq. (4)], isotherms were applied [32]. The adsorption process was performed at various metal ion concentrations, using a fixed amount of bionanocomposite. The range of Fe(III) and Pb(II) initial concentrations were 30–200 and 30–120 mg L^{-1} , respectively.

$$\frac{C_e}{q_e} = \frac{1}{q_m K_L} + \frac{C_e}{q_m} \quad (3)$$

$$\ln q_e = \ln K_F + \left(\frac{1}{n}\right) \ln C_e \quad (4)$$

Here, C_e (mg L^{-1}) and q_m (mg g^{-1}) are the equilibrium concentration of metal ions in the solution and the monolayer coverage capacity of adsorbent, respectively; K_L (L mg^{-1}) is the Langmuir constant; K_F [$(\text{mg g}^{-1}) (\text{L g}^{-1})^n$] is the Freundlich constant and n is the Freundlich exponent related to heterogeneity factor.

Photocatalytic Degradation Studies

The photocatalytic capability of the synthesized materials was analyzed by MB under visible light irradiation. The photocatalytic mixture was prepared by exploiting 0.5 gr L^{-1} as-prepared catalysts with 10 mL of aqueous MB solution at 20 mg L^{-1} concentration. After mechanically stirring in the dark for 30 min, the mixture achieved equilibrium. The suspension was then exposed to visible light under vigorous stirring. The irradiated sample was collected at various time intervals, and centrifuged at 4500 rpm for 10 min to get the supernatant. Then, dye concentration was measured by a UV–visible absorption spectrophotometer at 665 nm.

Results and Discussion

SEM and EDX Analysis

Figure 1a–h presents the SEM photographs of NCS, Bt, SnO₂-ZnO, and NCS/Bt/SnO₂-ZnO samples, respectively. As revealed in Fig. 1a and b, the NCS is quasi-spherical in morphology, and the surface area is rough. Figure 1c and d show the particles of the Bt in a sheet structure with a porous nature. The SEM image of the SnO₂-ZnO biosynthesized nanocomposite is demonstrated in Fig. 1e and f. The nanoparticles are aggregated most likely due to the calcination process. From the micrograph, Fig. 1g and h, it can be seen that the surface of the NCS/Bt/SnO₂-ZnO bionanocomposite is rough, with numerous protruding agglomerates, which is indicative of a large specific surface area and active sites. Also, a non-homogenous structure, with a very different morphology from those of initial materials (NCS, Bt, SnO₂-ZnO), is shown by the NCS/Bt/SnO₂-ZnO bionanocomposite. These results confirm that the NCS/Bt/SnO₂-ZnO is synthesized successfully, and it is a suitable candidate for the removal of contaminants.

Figure 2a–d shows the EDX spectra of samples to identify the elemental composition of materials. As can be seen in Fig. 2a, the EDX spectrum of the NCS demonstrates the

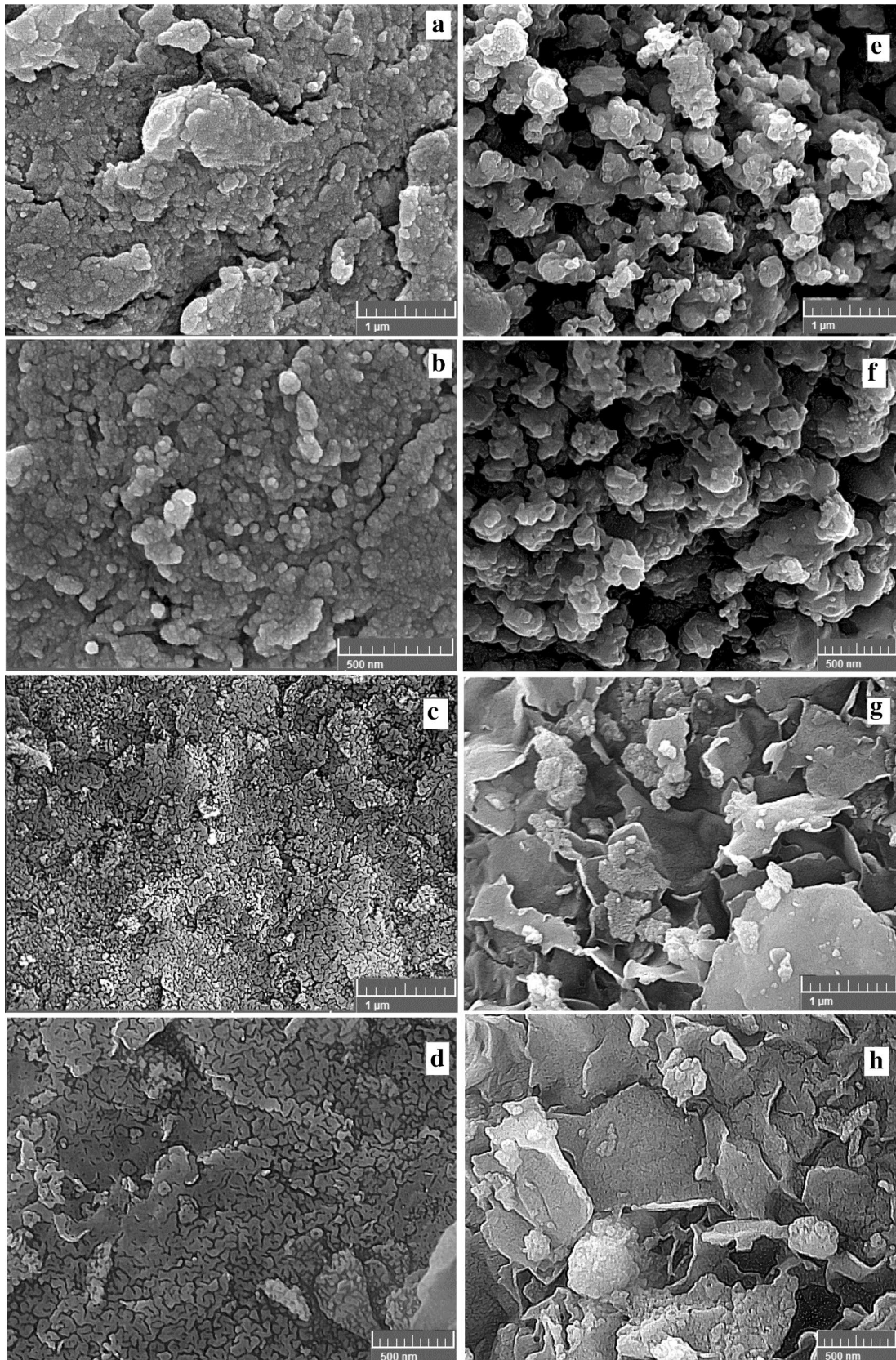


Fig. 1 FESEM micrographs of **a, b** NCS, **c, d** Bt, **e, f** SnO₂/ZnO, and **g, h** NCS/Bt/SnO₂/ZnO

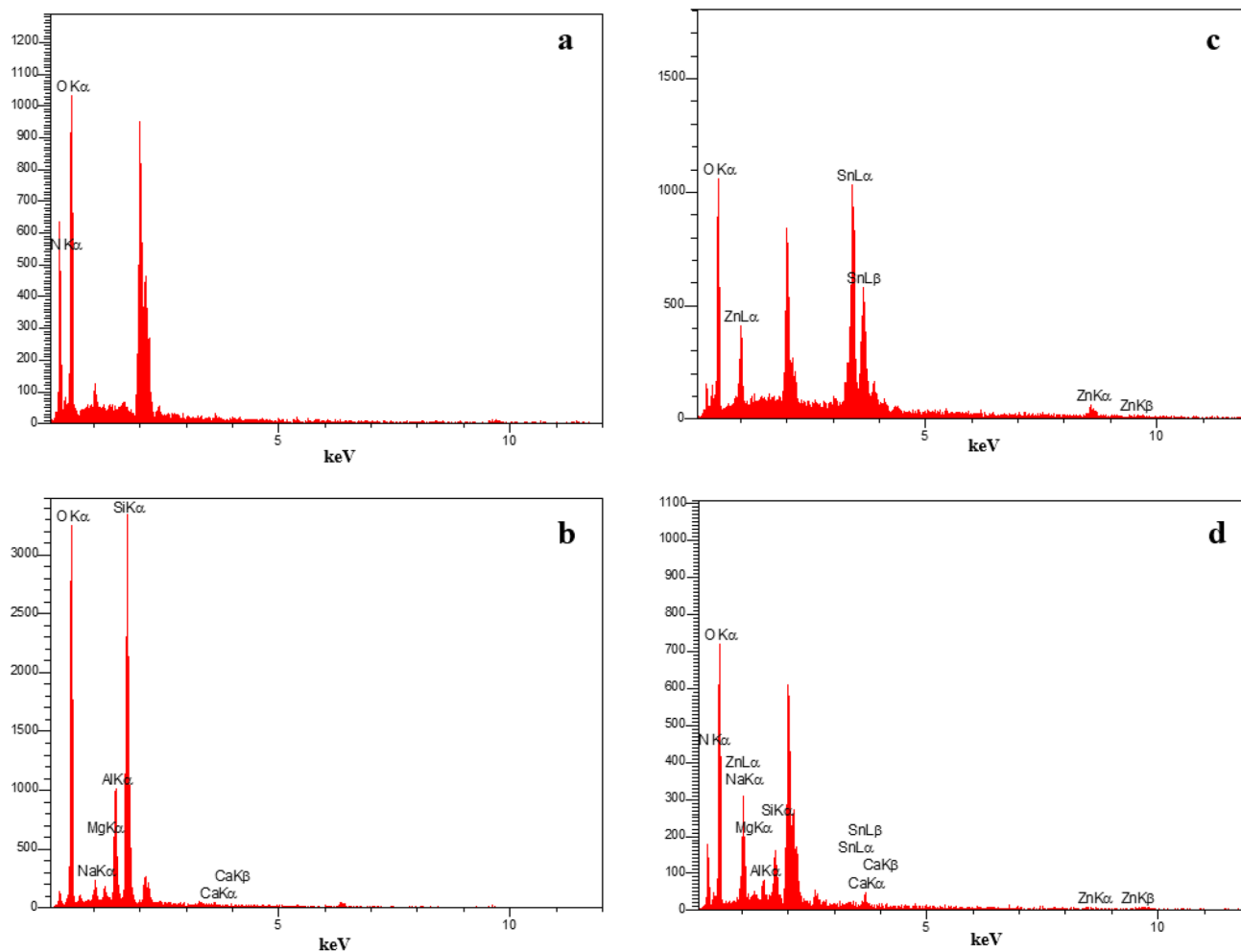


Fig. 2 EDX spectrum of **a** NCS, **b** Bt, **c** SnO₂/ZnO, and **d** NCS/Bt/SnO₂/ZnO

elements O, C, and N with wt% of 57.74, 27.04, and 15.22, respectively. Figure 2b reveals the composition of 63.47% O, 25.16% Si, 7.46% Al, 2.41% Na, 1.28% Mg, and 0.22% Ca in the Bt sample. The EDX analysis of the SnO₂–ZnO in Fig. 2c confirms that the nanocomposite contains the elements O, Sn, and Zn with wt% of 39.00, 39.97, and 21.04, respectively. In contrast, the NCS/Bt/SnO₂–ZnO bionanocomposite in Fig. 2d indicates the elements O, C, N, Na, Mg, Al, Si, Ca, Zn, and Sn with wt% of 44.51, 19.79, 9.64, 8.93, 0.69, 1.11, 2.86, 0.79, 6.13, and 5.55, respectively. The EDX analysis shows the successful formation of the NCS/Bt/SnO₂–ZnO bionanocomposite.

XRD Analysis

The XRD patterns of NCS, Bt, SnO₂–ZnO, and NCS/Bt/SnO₂–ZnO samples are exhibited in Fig. 3. The XRD spectrum of NCS Fig. 3a shows a broad peak at around $2\theta = 27^\circ$ which indicates that the crystallinity of NCS is low and

the polymer has the amorphous nature [9]. This demonstrates that NCS includes many reaction sites to enhance the removal performance of the final catalyst [33]. In the Bt spectrum Fig. 3b, the main diffraction peaks at 2θ values of 19.8° , 21.8° , 36.0° , and 62.5° can correspond to the (100), (105), (210), and (300) reflecting planes respectively. For SnO₂–ZnO Fig. 3c, the peaks at 2θ of 26.6° , 33.8° , 37.8° , 51.7° , and 65.4° can be indexed to the diffraction of the tetragonal phase of SnO₂ nanoparticles. In contrast, the characteristic peak at 2θ of 29.6° corresponds to the diffraction of the orthorhombic phase of the nanoparticles. The diffraction peaks at 2θ values of 31.5° , 47.6° , 56.2° , 62.4° , 67.3° , and 69.1° are attributed to the diffraction of the hexagonal phase of ZnO nanoparticles. These results exhibit that SnO₂–ZnO nanocomposite is successfully synthesized using the eco-friendly technique reported in this study. In the NCS/Bt/SnO₂–ZnO spectrum Fig. 3d, the broad peak of NCS at 26° vanished, and the intensity of diffraction peaks of Bt at 19.8° , 21.8° decreased, which indicates the existence of

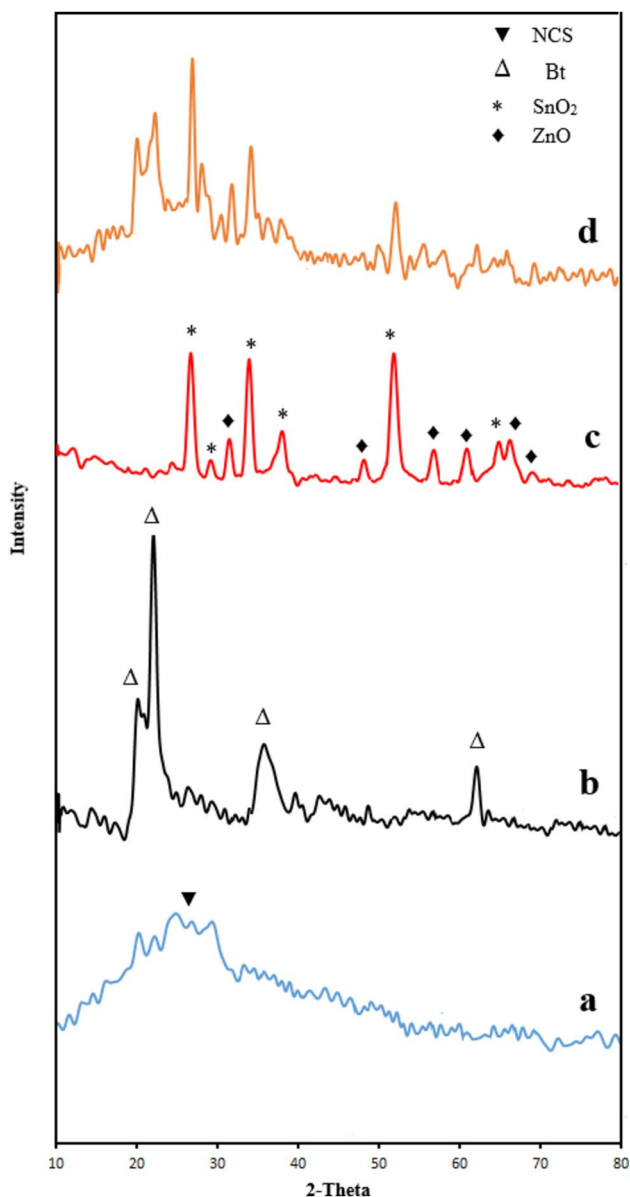


Fig. 3 XRD patterns of (a) NCS, (b) Bt, (c) SnO₂/ZnO, and (d) NCS/Bt/SnO₂/ZnO

strong interactions between NCS and Bt. Also, the related peaks to SnO₂ and ZnO nanoparticles appeared, which shows uniform dispersion of SnO₂-ZnO in the NCS/Bt network.

FTIR Analysis

Figure 4 shows (a) NCS, (b) Bt, (c) SnO₂-ZnO, and (d) NCS/Bt/SnO₂-ZnO FTIR spectra. In the spectrum of the NCS, the broad stretch band at 3424 cm⁻¹ is associated with the vibration of NH₂ and OH groups, while the peak at 2939 cm⁻¹ is due to the -C-H symmetric stretching mode. The bands observed at 1645 and 1547 cm⁻¹ corresponding

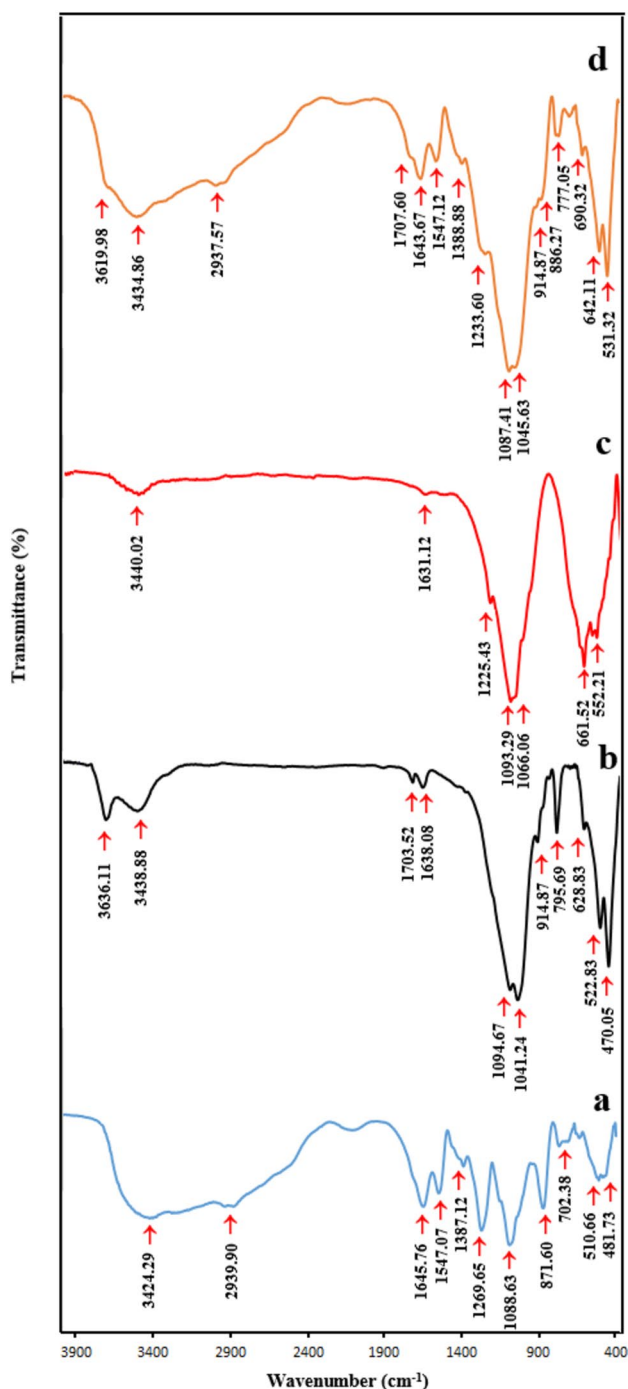


Fig. 4 FTIR spectrum of (a) NCS, (b) Bt, (c) SnO₂/ZnO, and (d) NCS/Bt/SnO₂/ZnO

to the CONH₂ and NH₂ groups, respectively, indicate the interaction between NH₃⁺ ions of chitosan and phosphate ions of TPP associated with the synthesis of NCS [9]. The band stated at 1387 cm⁻¹ is attributed to -CH₂ wagging, whereas the peaks at 1269 and 1088 cm⁻¹ are ascribed to P=O and P-O stretching modes of phosphate groups [33]. In the spectrum of Bt, the peak at 3636 cm⁻¹ corresponds

to Al–OH and Si–OH stretching vibrations, whereas the band 3438 cm^{-1} is ascribed to O–H and H–O–H stretching vibrations. The bands located at 1638 , 914 , and 522 cm^{-1} can be attributed to OH bending vibration in H–O–H, OH bending vibration in Al–Al–OH, and Si–O bending vibration in Si–O–Al, respectively. The peaks observed at 1041 and 795 cm^{-1} are due to Si–O–Si stretching vibration, and the band at 470 cm^{-1} is ascribed to the vibration mode of Si–O–Al [34]. The adsorption peak in the FTIR spectrum of SnO₂–ZnO at 3440 cm^{-1} is associated with the stretching mode of O–H of phenolic compounds, while the band at 1631 cm^{-1} is related to –OH bending vibration of water molecules existing in the nanocomposite. The intense peaks within the range of 900 – 1400 cm^{-1} are ascribed to the C–O vibration of *Salvia officinalis* extract [35]. The peaks observed at 552 , and 661 cm^{-1} are ascribed to the Zn–O and Sn–O stretching vibration modes, respectively [36]. These results confirm that SnO₂–ZnO was synthesized using *Salvia officinalis* extract as a natural capping agent. The FTIR spectrum of NCS/Bt/SnO₂–ZnO bionanocomposite exhibits the main characteristic bands recognized in NCS, Bt, and SnO₂–ZnO, which confirms the nanocomposite formation. The peak at 552 cm^{-1} , belonging to the Zn–O vibration mode in ZnO nanoparticles, shifts slightly to 531 cm^{-1} , while the band observed at 661 cm^{-1} , attributing to the Sn–O vibration mode in SnO₂ nanoparticles, shifts to 642 cm^{-1} . This shift in the peaks is due to the interaction between the NCS/Bt matrix and the SnO₂–ZnO nanocomposite [9, 34]. Also, the bonds at 3619 and 3434 cm^{-1} indicate that the surface functionalities of NCS/Bt/SnO₂–ZnO bionanocomposite, such as OH and NH, might play a significant role in the adsorption–photodegradation process [31].

TGA Analysis

To investigate the thermal stability of samples, TGA was carried out under an air atmosphere. The TGA curves of NCS, Bt, SnO₂–ZnO, and NCS/Bt/SnO₂–ZnO are represented in Fig. 5a–d. The TG curve of NCS Fig. 5a exhibits 6.89% weight loss in the range of 50 – $100\text{ }^{\circ}\text{C}$, mainly from the removal of structural water. The decomposition of the polymer matrix is initiated at $200\text{ }^{\circ}\text{C}$, and a weight loss of 33.10% occurs from 180 to $330\text{ }^{\circ}\text{C}$. Also, 23.90% weight loss with the temperature increasing from 700 to $900\text{ }^{\circ}\text{C}$ is observed. It corresponds to the disintegration of the chitosan backbone and conversion to volatile compounds with low molecular weight. At the end of the experiment, NCS exhibits weight loss of approximately 63.89%. In the TG curve of Bt Fig. 5b, the first weight loss of 3.83% at a temperature range of 40 – $100\text{ }^{\circ}\text{C}$ occurs due to the evaporation of water molecules adsorbed on the sample surfaces. The second stage, with a weight loss of 11.92% of the initial weight, is within the range of 400 – $900\text{ }^{\circ}\text{C}$, related

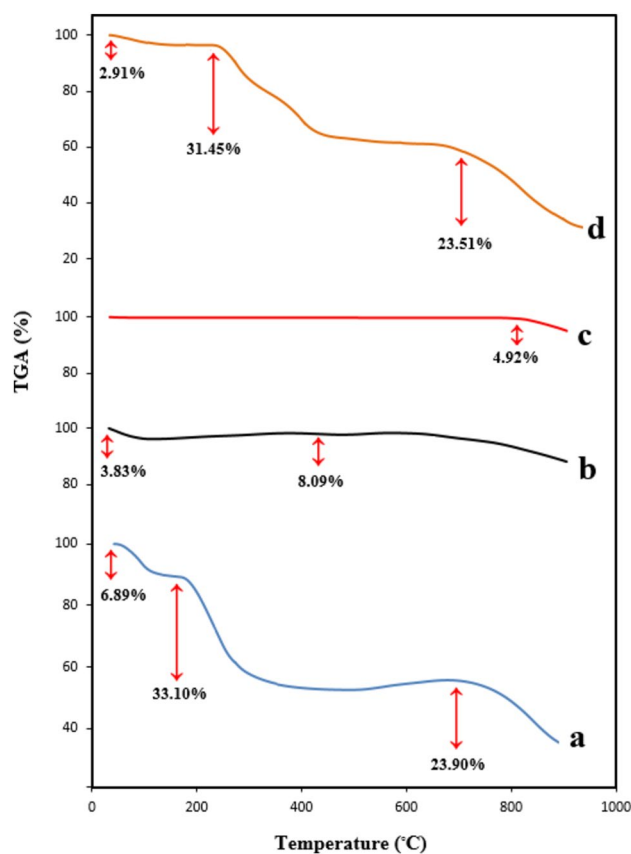


Fig. 5 TGA curves of (a) NCS, (b) Bt, (c) SnO₂/ZnO, and (d) NCS/Bt/SnO₂/ZnO

to the dehydroxylation of the aluminosilicate lattice. The SnO₂–ZnO nanocomposites Fig. 5c show a 4.92% weight loss between 800 and $900\text{ }^{\circ}\text{C}$, which is assigned to the formation of stable SnO₂ and ZnO nanoparticles and thermal decomposition of residual carbon components. As shown in Fig. 5d, the NCS/Bt/SnO₂–ZnO demonstrates a weight loss of 2.91% at a temperature range of 50 – $100\text{ }^{\circ}\text{C}$ due to dehydration. The weight loss at 220 – $450\text{ }^{\circ}\text{C}$ might be a result of depolymerization and deacetylation of the NCS in NCS/Bt/SnO₂–ZnO bionanocomposite, since SnO₂–ZnO nanoparticles and Bt are stable in this temperature range. According to the results in Fig. 5a and d, the TG analyses curves of NCS and NCS/Bt/SnO₂–ZnO, over the temperature ranging from 200 to $400\text{ }^{\circ}\text{C}$, are different, which indicates a difference in their degradation mechanism. Also, the TG analyses curve of NCS/Bt/SnO₂–ZnO appears late compared to that of NCS, confirming an improvement in its thermal stability. At about $300\text{ }^{\circ}\text{C}$, the weight loss for NCS and NCS/Bt/SnO₂–ZnO are 37.39%, and 22.54%, respectively. This trend indicates the existence of effective interactions between the functional groups of NCS and the SnO₂–ZnO nanoparticles and the silicate layer of Bt [34]. The third mass loss in the range of 680 – $900\text{ }^{\circ}\text{C}$ corresponds to the thermal decomposition of

NCS and elimination of volatile products, as well as to the dehydroxylation of the Bt lattice. Based on the results, the NCS/Bt/SnO₂-ZnO bionanocomposite, is thermally stable in the region of working temperature for the removal of heavy metal ions or degradation of dye.

DSC Analysis

To understand the thermal behavior of samples, the DSC analysis was performed. The DSC curves of NCS, Bt, SnO₂-ZnO, and NCS/Bt/SnO₂-ZnO are given in Fig. 6a–d. As shown in Fig. 6a, the endothermic peak at 75.38 °C can be ascribed to the dehydration of chitosan, while the exothermic peak at 203.23 °C corresponds to its degradation reaction. The DSC curve of Bt in Fig. 6b demonstrates an endothermic peak at 412.71 °C, which is assigned to the dehydroxylation of the mineral. Based on the DSC curve of NCS/Bt/SnO₂-ZnO in Fig. 6d, the endothermic and exothermic peaks were recorded at 82.20 °C and 443.15 °C, respectively. Based on the results, the glass transition temperature of NCS and NCS/Bt/SnO₂-ZnO were found to be 191.73 and 320.81 °C, respectively, which indicated the higher thermal stability of the prepared bionanocomposite.

UV-vis-DRS Analysis

The optical characteristics of SnO₂-ZnO and NCS/Bt/SnO₂-ZnO were analyzed by DRS. As seen in Fig. 7a, SnO₂-ZnO nanoparticles show good absorption in the UV region with a band gap of 3.15 eV. After the modification, the absorbance intensity of NCS/Bt/SnO₂-ZnO nanocomposite increases. Also, the nanocomposite exhibits a redshift in the absorption band, with a reduced band gap of 2.60 eV. It seems that the modification process has a significant influence on the band gap energy and the absorption band intensity of SnO₂-ZnO. As a result, the NCS/Bt/SnO₂-ZnO nanocomposite has high photocatalytic performance under the irradiation of visible light. This may be attributed to the interaction between NCS, Bt, and SnO₂-ZnO nanocomposites [34, 37].

BET Analysis

The specific surface area, pore size distribution, and pore volume of the prepared NCS/Bt/SnO₂/ZnO were determined by BET analysis. The results indicated that the bionanocomposite had a surface area of 32.54 m² g⁻¹, an average pore size of 17.98 nm, and a pore volume of 0.11 cm³ g⁻¹. These values suggest that the NCS/Bt/SnO₂/ZnO is typical of the mesoporous structure [38]. The large surface area and mesoscopic nature of the NCS/Bt/SnO₂/ZnO provide more surface reaction sites, which can be helpful for applications involving adsorption and photocatalytic degradation.

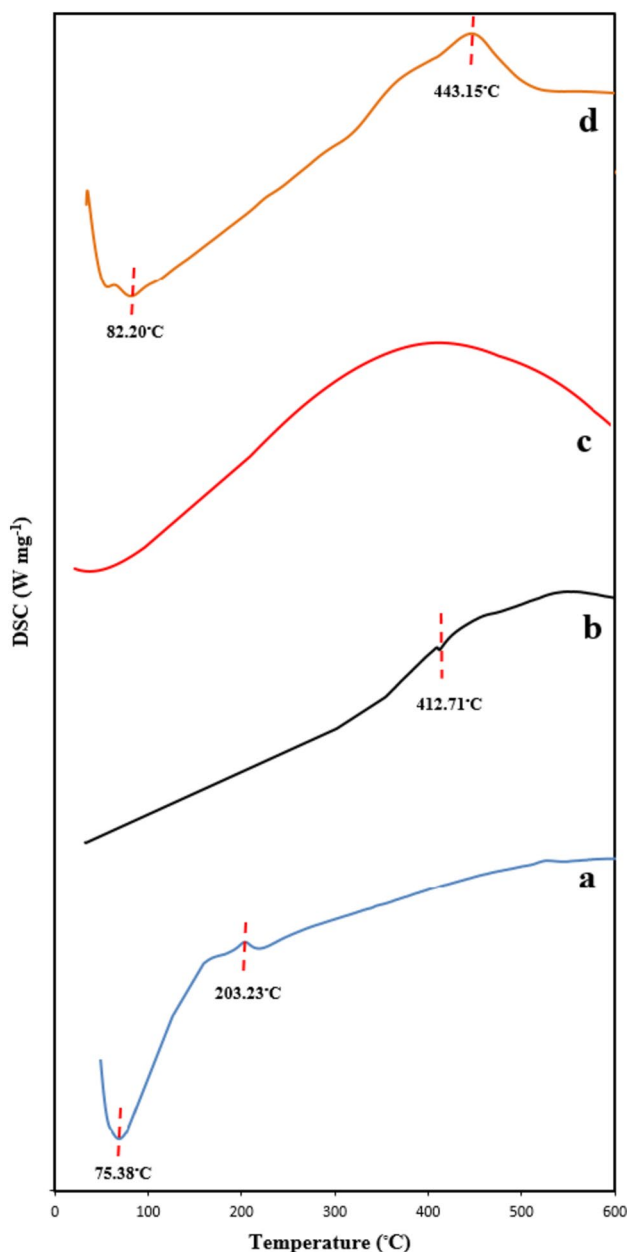


Fig. 6 DSC curves of (a) NCS, (b) Bt, (c) SnO₂/ZnO, and (d) NCS/Bt/SnO₂/ZnO

Heavy Metals Adsorption Behavior

The adsorption properties of NCS, Bt, SnO₂/ZnO, and NCS/Bt/SnO₂-ZnO on the removal of metal ions (Fe(III) and Pb(II)) were evaluated, and the results are depicted in Fig. 8a, b. Experiments were performed by adding 0.3 g L⁻¹ of adsorbent dosage into 10 mL of Fe(III) or Pb(II) solution, in which the ion concentration was 50 mg L⁻¹. The solutions pH of Fe(III) and Pb(II) was adjusted to 4.0, and 5.0, respectively. As depicted in Fig. 8a, approximately 64.4%, 75.3%, 83.1%, and 99.5% of Fe(III) was removed

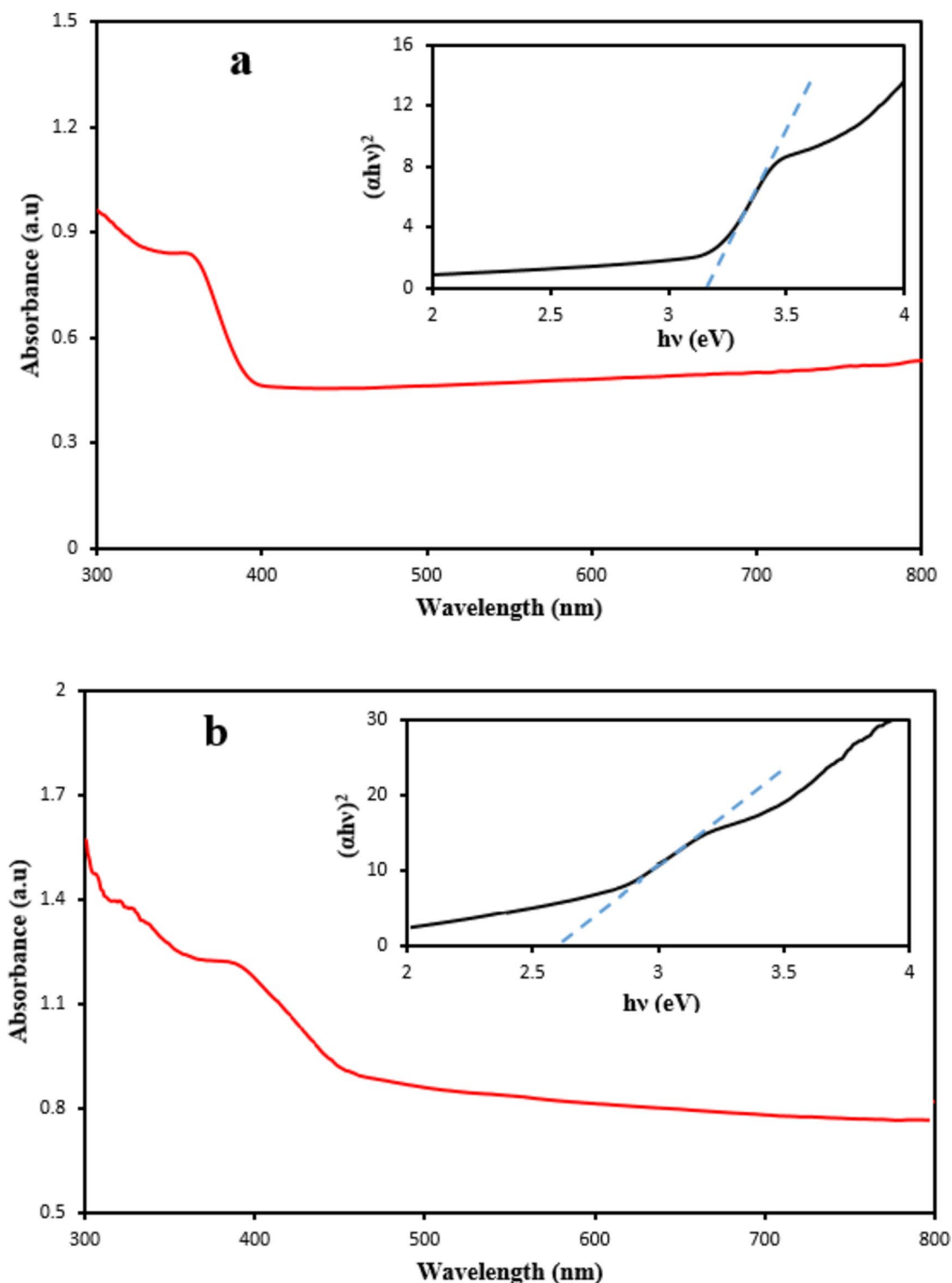
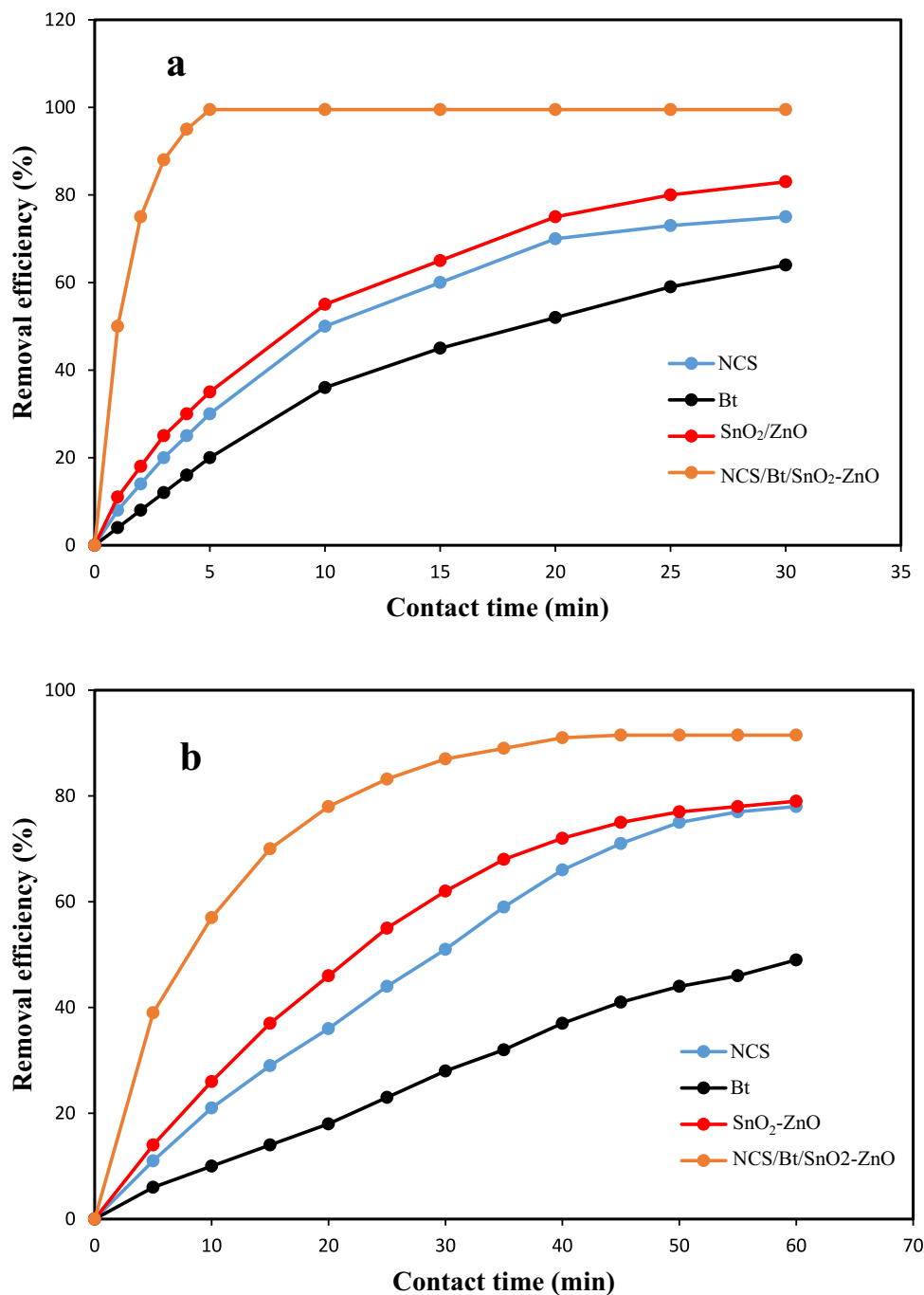


Fig. 7 UV-Vis DRS and Tauc's plot (inset) of **a** SnO₂/ZnO, and **b** NCS/Bt/SnO₂/ZnO

in 30 min by Bt, NCS, SnO₂-ZnO, and NCS/Bt/SnO₂-ZnO respectively. In fact, 99% of Fe(III) was removed in 5 min by NCS/Bt/SnO₂-ZnO bionanocomposite. This shows that the NCS/Bt/SnO₂-ZnO bionanocomposite effectively

removes Fe(III) with an excellent elimination rate. As shown in Fig. 8b, the Pb(II) removal efficiencies within 60 min were computed as 49.4%, 78.1%, 79.3%, and 91.5% for Bt, NCS, SnO₂-ZnO, and NCS/Bt/SnO₂-ZnO

Fig. 8 Removal of **a** Fe(II) and **b** Pb(II) over the different samples as a function of contact time



respectively. From the results, it can be considered that the removal of metal ions is significantly improved in the presence of NCS/Bt/SnO₂-ZnO biocomposite compared to NCS, Bt, SnO₂-ZnO. High removal efficiency and fast adsorption rates result from the large specific surface areas, active adsorption sites, and the porous nature of the NCS/Bt/SnO₂-ZnO. Therefore, the prepared bionanocomposite is a promising adsorbent of Fe(III) and Pb(II) for water treatment.

The Effect of pH

The pH influence on Fe(III) or Pb(II) removal efficiencies was investigated in the range of 1.0 to 7.0 while holding the NCS/Bt/SnO₂-ZnO dosage and initial metal ion concentration at fixed values of 0.2 g L⁻¹ and 50 mg L⁻¹, respectively. As depicted in Fig. 9a, b, the maximum efficiencies for the removal of Fe(III) and Pb(II) were observed at pH of 4.0 for Fe(III), and 5.0 for Pb(II), with values of 95.7% and 89.0%,

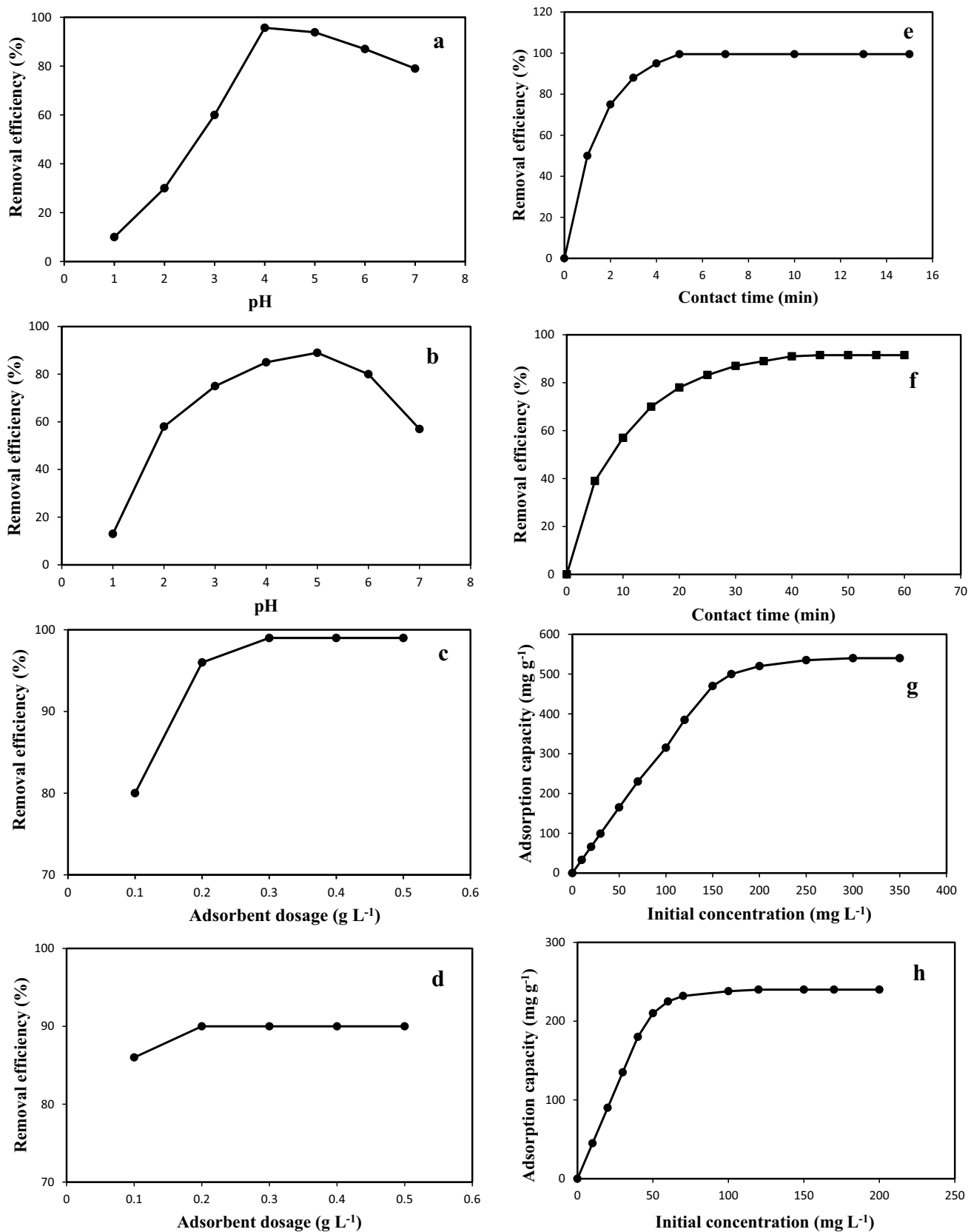


Fig. 9 Effect of pH **a, b**, adsorbent dosage **c, d**, contact time **e, f**, and initial metal ion concentration **g, h** on Fe(II) and Pb(II) removal using NCS/Bu/SnO₂/ZnO bionanocomposite

respectively. At strongly acidic solutions, the functional groups in the NCS/Bt/SnO₂-ZnO bionanocomposite were protonated and presented in the positively charged form, which will prevent Fe(III) and Pb(II) ions from approaching the surface of the bionanocomposite via electrostatic repulsion. When the pH is increased, the hydrogen ions concentration decreases, and more of the heavy metal ions could reach the surface of the composite and adsorb on it. Beyond pH of 4.0 (for Fe(III)) and pH 5.0 (for Pb(II)), precipitation of the heavy metal ions as the hydroxides might affect the decrease of metal adsorptions of NCS/Bt/SnO₂-ZnO bionanocomposite [39]. Thus, the optimal pH of 4.0 for Fe(III), and 5.0 for Pb(II) was selected to ensure the highest adsorption values and avoid precipitation of heavy metal ions.

The Effect of Adsorbent Dosage

The effect of NCS/Bt/SnO₂-ZnO dosage on the removal efficiency of Fe(III) and Pb(II) was investigated by adding various amounts of bionanocomposite from 0.1 to 0.5 g L⁻¹ into 10 mL of 50 mg L⁻¹ Fe(III) (pH 4.0) and Pb(II) (pH 5.0) solutions, respectively. As depicted in Fig. 9c, the Fe(III) adsorption efficiency increased from 80.0% to 99.0% with the increase of adsorbent amount from 0.1 to 0.3 g L⁻¹. This increment in removal efficiency could be related to the increase in the availability of reaction sites to remove Fe(III). After this optimum value, the removal efficiency remained constant due to the effect of NCS/Bt/SnO₂-ZnO adsorbent agglomeration, which diminished the surface active sites [31]. Thus, the optimum adsorbent dosage for removing Fe(III) was found to be 0.3 g L⁻¹. As observed in Fig. 9d, the removal efficiency of Pb(II) was increased from 86.0% to 90.0%, when the dosage of bionanocomposite was increased over the range of 0.1 g L⁻¹ to 0.2 g L⁻¹. For the dosage of NCS/Bt/SnO₂-ZnO bionanocomposite higher than 0.2 g L⁻¹, the Pb(II) adsorption efficiency remained constant. Therefore, the 0.2 g L⁻¹ of sorbent was used as the optimum dose of NCS/Bt/SnO₂-ZnO for Pb(II) adsorption on the bionanocomposite.

The Effect of Contact Time

Fe(III) and Pb(II) removal efficiency by NCS/Bt/SnO₂-ZnO was investigated as a function of adsorption time. As presented in Fig. 9e, the removal rate of Fe(III) was high, and the adsorption process reached equilibrium within 5 min. It was seen that the removal efficiency was over 99.5% at 5 min, which was superior to other reported adsorbents [40–42]. The fast Fe(III) removal could be ascribed to the abundance of adsorption vacant sites for interaction with metal ions, which resulted in the increment of the concentration gradient between Fe(III) ions and on the surface of the bionanocomposite. The influence of adsorption time on

the uptake of Pb(II) by bionanocomposite was illustrated in Fig. 9f. As shown, the Pb(II) adsorption efficiency increased sharply within 20 min, after that decreased gradually; finally, it reached maximum equilibrium in 40 min. The sharp rise in the initial adsorption period is attributed to the availability of adsorption sites for NCS/Bt/SnO₂-ZnO. With the increase of time, finding binding sites becomes difficult for Pb(II) ions, and the removal efficiency attains equilibrium eventually.

The Effect of Initial Concentration of Metal Ion

The impact of initial Fe(III) and Pb(II) concentration on the adsorption capacity was tested by altering the ions concentration in the range of 10–200 mg L⁻¹, and the results were shown in Fig. 9g, h. As presented in Fig. 9g, when the initial Fe(III) concentration was increased from 10 to 150 mg L⁻¹, the adsorption capacity of NCS/Bt/SnO₂-ZnO was increased from 50.0 mg g⁻¹ to 495.8 mg g⁻¹. This was due to the increasing driving force to transfer Fe(III) from the bulk solution onto the adsorbent. Higher amounts of initial Fe(III) concentration caused no significant increase in the adsorption capacity because of the saturation of adsorption sites of the bionanocomposite. According to Fig. 9h, the adsorption capacity of NCS/Bt/SnO₂-ZnO increased from 85.2 to 228.1 mg g⁻¹ with the initial Pb(II) concentration from 10 to 70 mg L⁻¹. The results indicated that the NCS/Bt/SnO₂-ZnO is effective in the removal of Fe(III) and Pb(II) with an excellent adsorption capacity.

Adsorption Kinetics

To understand the mechanism of Fe(III) and Pb(II) adsorption on NCS/Bt/SnO₂-ZnO, the pseudo-first-order and pseudo-second-order adsorption models were studied. The results are exhibited in Fig. 10a–d, and the kinetic parameters are tabulated in Table 1. As shown, the removal process followed the pseudo-second-order kinetics (Fe(III): R² = 0.9973, Pb(II): R² = 0.9937). Moreover, the theoretical q_e values obtained from pseudo-second-order kinetics agreed well with the experimental data. This fitting result suggested that the reaction rate was mainly determined by the chemisorption process on the heterogeneous adsorbent. According to the results, the adsorption rates of Fe(III) and Pb(II) at the beginning are fast, indicating the good affinity between adsorbent and adsorbates. Abundant functional groups, as well as the high surface area of the prepared NCS/Bt/SnO₂-ZnO bionanocomposite, cooperate to increase the removal efficiency. The possible mechanism of Fe(III) and Pb(II) adsorptions includes the transfer, sharing, or exchange of electrons between the metal ions and the surface functionalities of the bionanocomposite. For NCS/Bt/SnO₂-ZnO, the hydroxyl groups (–OH) or amine groups (–NH₂) in NCS and hydroxyl groups (e.g.,

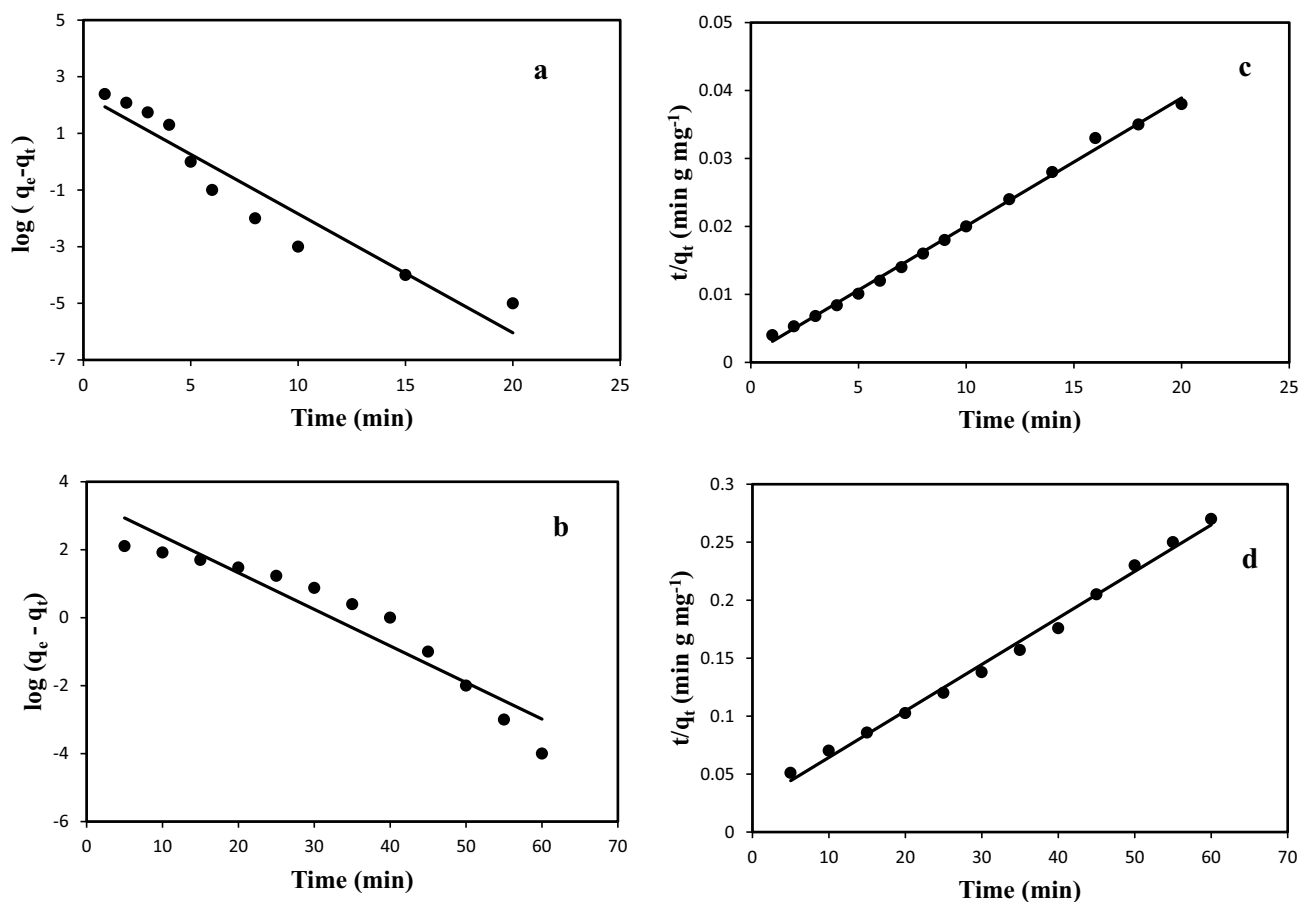


Fig. 10 The linear fitting of pseudo-First-order (a, b) and pseudo-second-order (c, d) plots for adsorption of Fe(III), and Pb(II) on NCS/Bt/SnO₂/ZnO bionanocomposite (pH: Fe(III) 4.0, Pb(II) 5.0; adsorbent

content: Fe(III) 3.0 g L⁻¹, Pb(II) 2.0 g L⁻¹; initial metal ion concentration: Fe(III) 150 mg L⁻¹, Pb(II) 50 mg L⁻¹)

Table 1 Kinetic parameters of Fe(III) and Pb(II) removal using NCS/Bt/SnO₂-ZnO

Contaminant	Experimental data		Pseudo-first order model		Pseudo-second order model		
	q _{e,exp} (mg g ⁻¹)	q _e (mg g ⁻¹)	k ₁ (min ⁻¹)	R ²	q _e (mg g ⁻¹)	k ₂ (× 10 ⁺³ g mg ⁻¹ min ⁻¹)	R ²
Fe(III)	540.012	228.454	0.967	0.914	526.316	3.008	0.997
Pb(II)	237.112	446.683	0.154	0.950	250.001	0.661	0.994

AlOH and SiOH) of Bt will ion-exchange with the heavy metal ions by replacing H⁺ by the electrostatic interaction [43, 44]. Furthermore, the functional groups of -NH₂ in NCS have coordinative chelation with Fe(III) and Pb(II) [43]. In addition, SnO₂ and ZnO nanoparticles, which are coated on the surface of the biocomposite by covalent and hydrogen bonds, play the main role in removing metal ions [45]. According to the results, the removal process can be generally divided into electrostatic attraction and surface complexation or ion exchange between Fe(III) and Pb(II) ions and the adsorbent.

Adsorption Isotherms

Adsorption isotherms describe the equilibrium relationship between the metal ions adsorbed on the surface of the adsorbent and unbound ions remaining in the bulk solution. They can also estimate the maximum adsorption capacity of the adsorbent. Therefore, adsorption isotherms are essential in the design of adsorption treatment systems. To study the adsorption behavior of NCS/Bt/SnO₂-ZnO, Langmuir and Freundlich isotherms were used. Figure 11 depicts the adsorption isotherms obtained for Fe(III) and

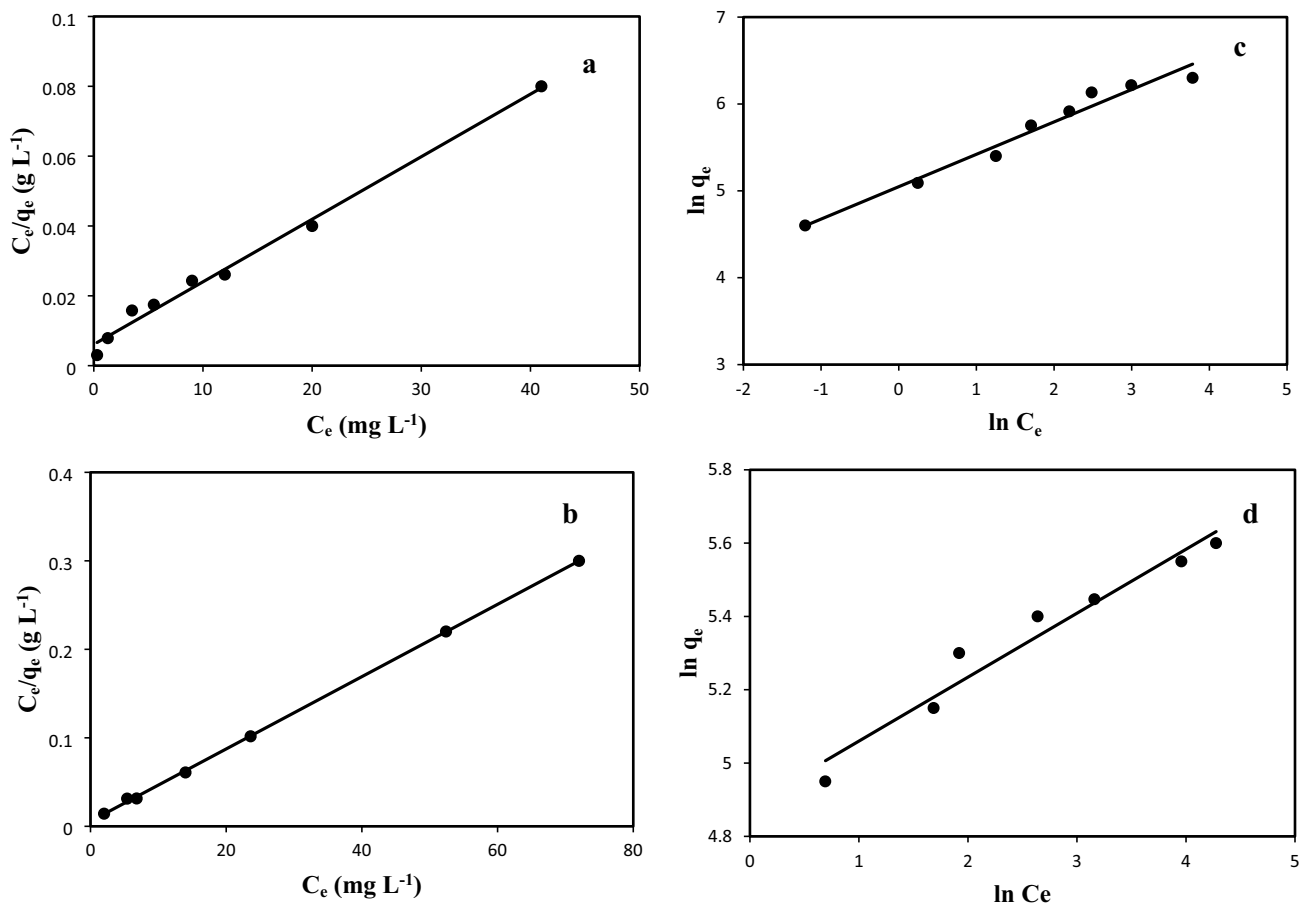


Fig. 11 Langmuir (a, b) and Freundlich (c, d) isothermal plots for adsorption of Fe(III), and Pb(II) on NCS/Bt/SnO₂/ZnO bionanocomposite (pH: Fe(III) 4.0, Pb(II) 5.0; adsorbent content: Fe(III) 3.0 g

L⁻¹, Pb(II) 2.0 g L⁻¹; initial metal ion concentration: Fe(III) 150 mg L⁻¹, Pb(II) 50 mg L⁻¹)

Pb(II) ions by NCS/Bt/SnO₂-ZnO and calculated isotherm data are given in Table 2. By comparing the coefficients of determination (R^2), the conclusion that could be drawn is that the adsorption data fit the Langmuir model better than the Freundlich model for the removal processes of both Fe(III) and Pb(II), suggesting that the adsorption of heavy metal ions onto NCS/Bt/SnO₂-ZnO is a monolayer process and the adsorbed ions do not interact [46]. For the confirmation of the favorability of the adsorption process, a separation factor constant [R_L , Eq. (5)] was calculated.

$$R_L = \frac{1}{1 + C_i K_L} \quad (5)$$

where K_L and C_i are the Langmuir equilibrium constant and initial concentration of metal ions, respectively. The values of R_L were found in the range of 0.017–0.102 for Fe(III), and 0.044–0.011 for Pb(II), showing that the adsorption of heavy metal ions on NCS/Bt/SnO₂-ZnO was desirable, which was further supported by the $1/n$ values less than 1 in the Freundlich isotherm. Moreover, the Langmuir values of the highest monolayer adsorption capacity (q_m) of Fe(III) and Pb(II) were 555.55 and 243.90 mg g⁻¹, respectively, which

Table 2 Adsorption isotherm parameters of Fe(III) and Pb(II) removal using NCS/Bt/SnO₂-ZnO

Contaminant	Langmuir			Freundlich		
	q_m (mg g ⁻¹)	K_L (L mg ⁻¹)	R^2	K_F (mg g ⁻¹)	n (L g ⁻¹)	R^2
Fe(III)	555.555	0.295	0.991	155.664	2.682	0.970
Pb(II)	243.902	0.719	0.999	132.357	5.734	0.952

was close to the experimental data. Table 3 compares the Fe(III) and Pb(II) adsorption capacity with other reported adsorbents [40–42, 47–51]. It is revealed that the adsorption capacity of NCS/Bt/SnO₂-ZnO was higher than most of the previously reported adsorbents. Also, the adsorbent used in this work was prepared by a green, cost-efficient, and simple method without using expensive or toxic reagents or solvents. These results suggest that NCS/Bt/SnO₂-ZnO is a practical and economically feasible biosorbent for industrial wastewater treatment.

The Photocatalytic Degradation of MB Dye

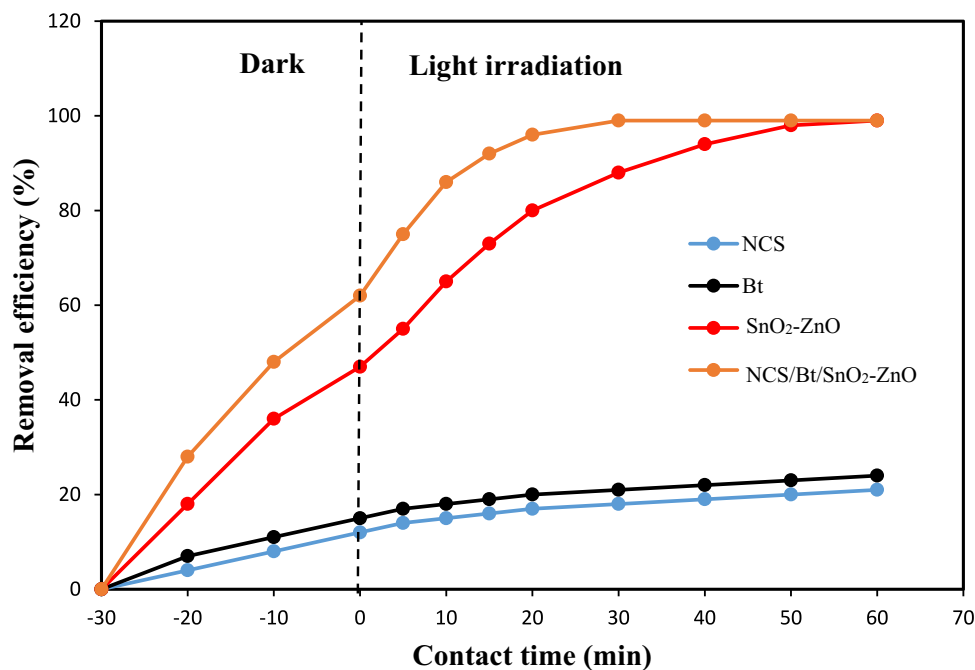
In the present study, the removal efficiency of the NCS/Bt/SnO₂-ZnO bionanocomposite was compared with the NCS,

Bt, SnO₂/ZnO for photodegradation of MB under the visible light and the results were presented in Fig. 12. From the dark results (the first 30 min), it could be concluded that the photocatalytic efficiency of MB was significantly improved in the presence of NCS/Bt/SnO₂-ZnO by comparison with NCS, Bt, SnO₂/ZnO. The removal efficiency of MB for the NCS/Bt/SnO₂-ZnO approached 62%, while NCS, Bt, and SnO₂/ZnO revealed 12%, 15%, and 47% of removal efficiency, respectively. The significant improvement of MB adsorption by NCS/Bt/SnO₂-ZnO could be attributed to the strong interactions between the hydroxyl (–OH), amine (–NH₂) or carbonyl (C=O) groups in NCS and the aluminosilicate structure of Bt (Al³⁺ and Si⁴⁺), as well as between the –NH₂, and –OH groups of NCS and SnO₂ and ZnO nanoparticles. Under visible light irradiation, NCS/Bt/SnO₂-ZnO

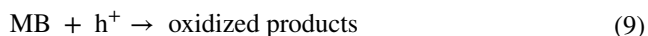
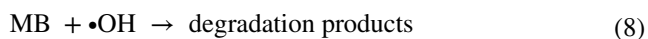
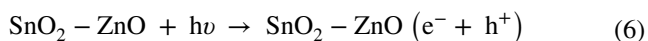
Table 3 Comparison of adsorption capacity of Fe(III) and Pb(II) on various adsorbents

Adsorbent	Surface area (m ² g ⁻¹)	pH		Contact time (min)		Adsorption capacity (mg g ⁻¹)		References
		Fe(III)	Pb(II)	Fe(III)	Pb(II)	Fe(III)	Pb(II)	
CTPP	–	3	–	60	–	13.72	–	[40]
PYCS	–	2.5	–	720	–	66.20	–	[41]
montmorillonite	19.8	4	–	300	–	28.9	–	[42]
TR/PAA	–	2.5	5	60	2	94.88	253.16	[47]
KB/Zn-Fe	31.30	–	5.5	–	720	–	161.29	[48]
Bentonite	31.36	–	7	–	120	–	27.23	[49]
Guar gum/bentonite	5.533	–	5.1	–	240	–	72.5	[50]
HDTMA-bentonite	19.82	–	5	–	120	–	25.8	[51]
NCS/Bt/SnO ₂ -ZnO	32.54	4	5	5	40	555.55	243.90	[This work]

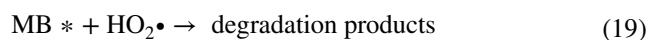
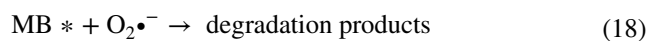
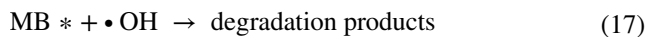
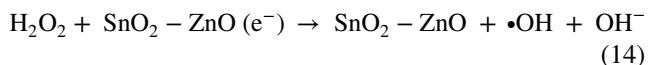
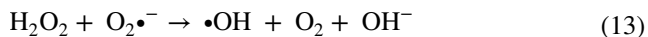
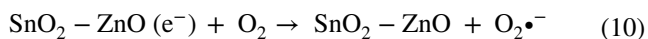
Fig. 12 Photocatalytic degradation **a** and kinetic plots of photocatalytic degradation **b** of SnO₂/ZnO and NCS/Bt/SnO₂/ZnO bionanocomposite for MB dye



showed 99% photodegradation after 30 min, while NCS, Bt, and SnO₂/ZnO exhibited 18%, 21%, and 88% of photocatalytic efficiency, respectively. It was clear that NCS/Bt/SnO₂-ZnO revealed the improvement of MB photocatalytic degradation compared to that of SnO₂-ZnO. According to the DRS results, the high photocatalytic activity of the NCS/Bt/SnO₂-ZnO could be attributed to the decrease of the band gap (2.73 eV) compared with SnO₂-ZnO (3.12 eV). Based on the experimental data, NCS/Bt/SnO₂-ZnO shows excellent performance efficiency due to the synergistic effects of adsorption and photocatalysis activity. Due to the large specific surface areas, active adsorption sites, and the porous nature of the NCS/Bt/SnO₂-ZnO, the MB molecules are efficiently adsorbed on the surface of the nanocomposite to establish the adsorption/desorption equilibrium. Under visible light irradiation, electron-hole pairs (e⁻ + h⁺) are generated in the SnO₂-ZnO nanocomposites [30, 31]. The holes react with OH⁻ of H₂O and produce a •OH radical or directly oxidize MB dye molecule to degradation products.



However, the photogenerated electrons react with oxygen molecules present on the surface of the catalyst, creating superoxide and hydroxyl radicals. These radicals can degrade MB dye.



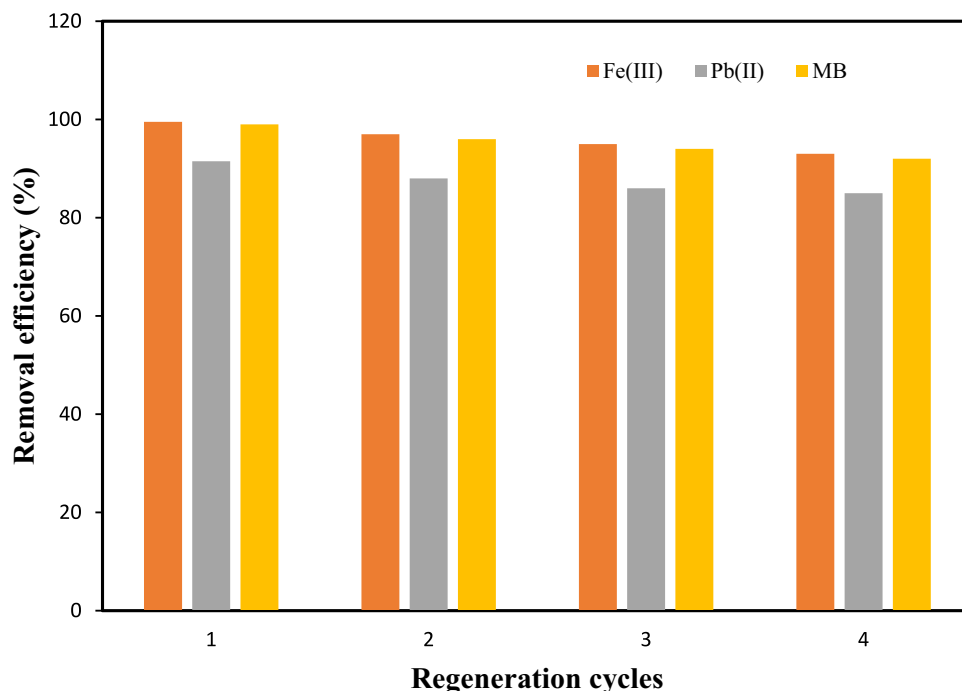
Regeneration and Recycling of NCS/Bt/SnO₂/ZnO

To assess the stability and reusability of the NCS/Bt/SnO₂/ZnO, cycling tests were performed. The used bionanocomposite was separated from the reaction solution by centrifugation and then was washed thoroughly with deionized water to reuse. As can be seen in Fig. 13, the removal performance of this bionanocomposite was preserved after four continuous cycles without any substantial reduction in removal activity (93.4% removal efficiency of Fe(III), 85.6% removal efficiency of Pb(II) and 92.2% removal efficiency of MB dye). Thus, the NCS/Bt/SnO₂/ZnO, with excellent renewability and reusability, is an economical and efficient material in practical wastewater treatment.

Conclusion

This work demonstrated the successful synthesis of NCS/Bt/SnO₂-ZnO bionanocomposite by a simple and cost-efficient green method for heavy metal ions and dye removal from aqueous media. Bionanocomposite comprised Nanochitosan (NCS), Bentonite (Bt), and SnO₂-ZnO nanocomposite prepared using *Salvia officinalis* extract as a reducing/stabilizing agent. The surface morphology of the as-prepared NCS/Bt/SnO₂-ZnO bionanocomposite showed a rough surface with porous nature, which was determined by FESEM. EDX, XRD, and FTIR results confirmed the formation of the NCS/Bt/SnO₂-ZnO nanocomposite. TGA data revealed an increase in the thermal stability of the NCS/Bt/SnO₂-ZnO compared to NCS. DRS results indicated that the band gap of SnO₂-ZnO was reduced by adding NCS and Bt. The surface area of NCS/Bt/SnO₂-ZnO was found to be 32.54 m² g⁻¹ with a 17.98 nm pore size. Due to the porous nature and abundant active adsorption sites, the NCS/Bt/SnO₂-ZnO bionanocomposite showed excellent performance in the removal of Fe(III) and Pb(II) from water. Under optimal conditions, the highest removal of Fe(III) (99.5%) and Pb(II) (91.5%) was achieved after 5 min and 40 min, respectively. By pseudo-second-order kinetic model, the values of the adsorption kinetic data were determined. The adsorption data fitted the Langmuir isotherm and indicated the removal capacity of 555.55 and 243.90 mg g⁻¹ for Fe(III) and Pb(II), respectively. NCS/Bt/SnO₂-ZnO was also used as an efficient photocatalyst for the degradation of MB in aqueous solutions. The results showed a dye degradation efficiency of 99% within 30 min. Moreover, the NCS/Bt/

Fig. 13 The removal efficiency of Fe(III), Pb(II) and MB on NCS/Bt/SnO₂/ZnO bionanocomposite during four regeneration cycles



SnO₂–ZnO could be utilized as a stable and reusable material for the removal of Fe(III), Pb(II), and MB from water. With simple operation and synthesized by inexpensive and environmentally friendly materials and a green synthesis route, as well as the excellent removal ability, the NCS/Bt/SnO₂–ZnO bionanocomposite might be practically useful as a proficient adsorbent/photocatalyst in pollutants removal from the wastewater. Furthermore, this report is expected to expand the scope of biological synthesis of other nanocomposites for practical uses.

Acknowledgements The authors acknowledge the financial support of this work by University of Torbat-e Jam, Torbat-e Jam, Iran.

Author Contributions Conceptualization, Methodology, Investigation, Data curation, Visualization, Validation, Writing- Reviewing and Editing: S.H.; Investigation: M.M.

Funding The authors have not disclosed any funding.

Declarations

Competing Interests The authors have not disclosed any competing interests.

References

- Singh A, Bahadur Pal D, Mohammad A, Alhazmi A, Haque S, Yoon T, Srivastava N, Kumar Gupta V (2022) Biological remediation technologies for dyes and heavy metals in wastewater treatment: new insight. *Bioresour Technol* 343:126154
- Heydari S, Eshagh Ahmadi S (2023) Synergistic adsorption-photocatalytic degradation of methyl green by magnetic Fe₃O₄/CMC@Cysteine-ZnO nanocomposite. *J Inorg Organomet Polym Mater* 33:1969–1982
- Zhao X, Baharinikoo L, Davoodabadi Farahani M, Mahdizadeh B, Kazemzadeh Farizhandi AA (2022) Experimental modelling studies on the removal of dyes and heavy metal ions using ZnFe₂O₄ nanoparticles. *Sci Rep* 12:5987
- Heydari S, Eshagh Ahmadi S (2023) Fabrication and characterization of polymer based magnetic dialdehyde carboxymethyl cellulose/cysteine nanocomposites for methylene blue removal. *Polym Bull* 80:3857–3882
- Chkirida S, Zari N, Bouhfid R, Qaiss A (2021) Insight into the bionanocomposite applications on wastewater decontamination: review. *J Water Process Eng* 43:102198
- Baruah R, Goswami M, Moni Das A, Nath D, Talukdar K (2023) Multifunctional ZnO bionanocomposites in the treatment of polluted water and controlling of multi-drug resistant bacteria. *J Mol Struct* 1283:135251
- Azmana M, Mahmood S, Hilles AR, Rahman A, Arifin MAB, Ahmed S (2021) A review on chitosan and chitosan-based bionanocomposites: promising material for combatting global issues and its applications. *Int J Biol Macromol* 185:832–848
- Tandekar S, Korde S, Saravanan D, Jugade R (2022) Gamma degraded oligomeric nanochitosan for adsorptive removal of Cd(II). *Bioresour Technol Rep* 18:101002
- El-saied H-A, Ibrahim AM (2020) Effective fabrication and characterization of eco-friendly nano chitosan capped zinc oxide nanoparticles for effective marine fouling inhibition. *J Environ Chem Eng* 8:103949
- Kausar A, Shahzad R, Iqbal J, Muhammad N, Ibrahim SM, Iqbal M (2020) Development of new organic-inorganic, hybrid bionanocomposite from cellulose and clay for enhanced removal of Drimarine Yellow HF-3GL dye. *Int J Biol Macromol* 149:1059–1071
- Alcantara ACS, Darder M, Aranda P, Ruiz-Hitzky E (2014) Polysaccharide-fibrous clay bionanocomposites. *Appl Clay Sci* 96:2–8

12. Ahmad R, Ejaz MO (2023) Efficient adsorption of crystal violet (CV) dye onto benign chitosan-modified L-cysteine/bentonite (CS-Cys/Bent) bionanocomposite: synthesis, characterization and experimental studies. *Dyes Pigm* 216:111305
13. Xu D, Kong Q, Wang X, Lou T (2022) Preparation of carboxymethyl cellulose/chitosan-CuO giant vesicles for the adsorption and catalytic degradation of dyes. *Carbohydr Polym* 291:119630
14. Stuparu Cretu M, Braniste G, Necula GA, Stanciu S, Stoica D, Stoica M (2023) Metal oxide nanoparticles in food packaging and their influence on human health. *Foods* 12:1882
15. Ghosh N, Das S, Biswas G, Haldar PK (2022) Review on some metal oxide nanoparticles as effective adsorbent in wastewater treatment. *Water Sci Technol* 85:3370–3395
16. Ionel Șerban I, Enesca A (2020) Metal oxides-based semiconductors for biosensors applications. *Front Chem* 8:354
17. Kotrange H, Najda A, Bains A, Robert Gruszecki R, Prince Chawla P, Tosif MM (2021) Metal and metal oxide nanoparticle as a novel antibiotic carrier for the direct delivery of antibiotics. *Int J Mol Sci* 22:9596
18. Yu S, Wang J, Cui J (2020) Preparation of a novel chitosan-based magnetic adsorbent CTS@SnO₂@Fe₃O₄ for effective treatment of dye wastewater. *Int J Biol Macromol* 156:1474–1482
19. Honarmand M, Mirzadeh M, Honarmand M (2020) Green synthesis of SnO₂-ZnO-eggshell nanocomposites and study of their application in removal of mercury (II) ions from aqueous solution. *J Environ Health Sci Eng* 18:1581–1593
20. Zarei S, Hasheminasari M, Masoudpanah SM, Javadpour J (2022) Photocatalytic properties of ZnO/SnO₂ nanocomposite films: role of morphology. *J Mater Res Technol* 17:2305–2312
21. Bukhari A, Ijaz I, Gilani E, Nazir A, Zain H, Saeed R, Alarfaji SS, Hussain S, Aftab R, Naseer Y (2021) Green synthesis of metal and metal oxide nanoparticles using different plants' parts for antimicrobial activity and anticancer activity: a review article. *Coatings* 11:1374
22. Varadavenkatesan T, Pai S, Vinayagam R, Selvaraj R (2021) Characterization of silver nano-spheres synthesized using the extract of *Arachis hypogaea* nuts and their catalytic potential to degrade dyes. *Mater Chem Phys* 272:125017
23. Heydari S, Hosseinpour Zaryabi M (2018) Response surface methodology for optimization of green silver nanoparticles synthesized via *Phlomis Cancellata* Bunge extract. *Anal Bioanal Chem* 5:373–386
24. Vinayagam R, Pai S, Varadavenkatesan T, Pugazhendhi A, Selvaraj R (2023) Characterization and photocatalytic activity of ZnO nanoflowers synthesized using *Bridelia retusa* leaf extract. *Appl Nanosci* 13:493–502
25. Saini R, Kumar P (2023) Green synthesis of TiO₂ nanoparticles using *Tinospora cordifolia* plant extract & its potential application for photocatalysis and antibacterial activity. *Inorg Chem Commun* 156:111221
26. Shet VB, Kumar PS, Vinayagam R, Selvaraj R, Vibha C, Rao S, Pawan SM, Poorvika G, Quintero VM, Ujwal P, Rajesh KS, Dubey A, Yumnam S (2023) Cocoa pod shell mediated silver nanoparticles synthesis, characterization, and their application as nanocatalyst and antifungal agent. *Appl Nanosci* 13:4235–4245
27. Vinayagam R, Kandati S, Murugesan G, Goveas LC, Baliga A, Pai S, Varadavenkatesan T, Kaviyarasu K, Selvaraj R (2023) Bioinspiration synthesis of hydroxyapatite nanoparticles using eggshells as a calcium source: evaluation of Congo red dye adsorption potential. *J Mater Res Technol* 22:169–180
28. Atri A, Echabaane M, Bouzidi A, Harabi I, Soucase BM, Ben Chaabane R (2023) Green synthesis of copper oxide nanoparticles using *Ephedra Alata* plant extract and a study of their antifungal, antibacterial activity and photocatalytic performance under sunlight. *Heliyon* 9:13484
29. Sri devi H, Ramananda Bhat M, Senthil Kumar P, Manoj Kumar N, Selvaraj R (2023) Structural characterization of cuboidal α -Fe₂O₃ nanoparticles synthesized by a facile approach. *Appl Nanosci* 13:5605–5613
30. Shdied S, Albeladi R, Ahmad Malik M, Ahmed Al-thabaiti S (2020) Facile biofabrication of silver nanoparticles using *Salvia officinalis* leaf extract and its catalytic activity towards Congo red dye degradation. *J Mater Res Technol* 9:10031
31. Sugashini S, Gomathi T, Aruna Devi R, Sudha PN, Rambabu K, Banat F (2022) Nanochitosan/carboxymethyl cellulose/TiO₂ biocomposite for visible-light-induced photocatalytic degradation of crystal violet dye. *Environ Res* 204:112047
32. Heydari S, Zare L, Eshagh Ahmadi S (2021) Removal of phenolphthalein by aspartame functionalized dialdehyde starch nanocomposite and optimization by Plackett–Burman design. *J Iran Chem Soc* 18:3417
33. Saranya M, Latha S, Gopal Reddi MR, Gomathi T, Sudha PN, Anil S (2017) Adsorption studies of lead(II) from aqueous solution onto nanochitosan/polyurethane /polypropylene glycol ternary blends. *Int J Biol Macromol* 104:1436
34. Aadnan I, Zegaoui O, El Mragui A, Esteves da Silva JCG (2022) Physicochemical and photocatalytic properties under visible light of ZnO-bentonite/chitosan hybrid-biocomposite for water remediation. *Nanomaterials* 12:102
35. Golmohammadi M, Nabipour Hassankiadeh M, Zhang L (2021) Facile biosynthesis of SnO₂/ZnO nanocomposite using *Acroptilon repens* flower extract and evaluation of their photocatalytic activity. *Ceram Int* 47:29303
36. Sayadi MH, Ghollasimood S, Ahmadpour N, Homaeigohar S (2022) Biosynthesis of the ZnO/SnO₂ nanoparticles and characterization of their photocatalytic potential for removal of organic water pollutants. *J Photochem Photobiol A* 425:113662
37. Aadnan I, Zegaoui O, Daou I, Esteves da Silva JCG (2020) Synthesis and physicochemical characterization of a ZnO-Chitosan hybrid-biocomposite used as an environmentally friendly photocatalyst under UV-A and visible light irradiations. *J Environ Chem Eng* 8:104260
38. Bhole R, Gonsalves D, Murugesan G, Narasimhan MK, Srinivasan NR, Dave N, Varadavenkatesan T, Vinayagam R, Govarthanan M, Selvaraj R (2023) Superparamagnetic spherical magnetite nanoparticles: synthesis, characterization and catalytic potential. *Appl Nanosci* 13:6003–6014
39. Ngamsurach P, Namwongsa N, Praipipat P (2022) Synthesis of powdered and beaded chitosan materials modified with ZnO for removing lead (II) ions. *Sci Rep* 12:17184
40. Ma A-M, López-Cervantes J, Sánchez-Machado DI, Sánchez-Duarte RG, Rodríguez-Núñez JR, Núñez-Gastélum JA (2012) Fe(II) and Fe(III) adsorption by chitosan-tripolyphosphate beads: kinetic and equilibrium studies. *J Water Supply Res T* 61:331–341
41. Zhang L, Liu H, Zhu J, Liu X, Li L, Huang Y, Fu B, Fan G, Wang Y (2023) Effective removal of Fe (III) from strongly acidic wastewater by pyridine-modified chitosan: synthesis, efficiency, and mechanism. *Molecules* 28:3445
42. Bhattacharyya KG, Gupta SS (2008) Kaolinite and montmorillonite as adsorbents for Fe(III), Co(II) and Ni(II) in aqueous medium. *Appl Clay Sci* 41:1–9
43. Gamage A, Jayasinghe N, Thiviya P, Wasana MLD, Merah O, Madhujith T, Koduru JR (2023) Recent application prospects of chitosan based composites for the metal contaminated wastewater treatment. *Polymers (Basel)* 15(6):1453
44. Amutenya ELM, Zhou F, Liu J, Long W, Ma L, Liu M, Lv G (2022) Preparation of humic acid-bentonite polymer composite: a heavy metal ion adsorbent. *Heliyon* 8:e09720
45. Honarmand M, Amini M, Arman Iranfar A, Naeimi A (2022) Green synthesis of ZnO/SnO₂ nanocomposites using pine leaves

- and their application for the removal of heavy metals from aqueous media. *J Clust Sci* 33:301–310
46. Heydari S (2021) Development of aspartame functionalized magnetic polymer nanocomposites for the zinc (II) removal from aqueous solution. *Iran J Sci Technol Trans Sci* 45:1311
 47. Zhang S, Liu C, Yuan Y, Fan M, Zhang D, Wang D, Xu Y (2020) Selective, highly efficient extraction of Cr(III), Pb(II) and Fe(III) from complex water environment with a tea residue derived porous gel adsorbent. *Bioresour Technol* 311:123520
 48. Tan Y, Wan X, Zhou T, Wang L, Yin X, Ma A, Wang N (2022) Novel Zn–Fe engineered kiwi branch biochar for the removal of Pb(II) from aqueous solution. *J Hazard Mater* 424:127349
 49. Li G, Liu X, Zhang J, Liu J, Yang Y (2022) Investigation of the adsorption characteristics of Pb(II) onto natural kaolinite and bentonite clays. *Desalin Water Treat* 262:121–136
 50. Ahmad R, Mirza A (2018) Synthesis of Guar gum/bentonite a novel bionanocomposite: Isotherms, kinetics and thermodynamic studies for the removal of Pb (II) and crystal violet dye. *J Mol Liq* 249:805–814
 51. Dinh VP, Nguyen PT, Tran MC, Luu AT, Hung NQ, Luu TT, Kiet HAT, Mai XT, Luong TB, Nguyen TL, Ho HTT, Nguyen DK, Pham DK, Hoang AQ, Le VT, Nguyen TC (2022) HTDMA-modified bentonite clay for effective removal of Pb(II) from aqueous solution. *Chemosphere* 286:131766

Publisher's Note Springer Nature remains neutral with regard to jurisdictional claims in published maps and institutional affiliations.

Springer Nature or its licensor (e.g. a society or other partner) holds exclusive rights to this article under a publishing agreement with the author(s) or other rightsholder(s); author self-archiving of the accepted manuscript version of this article is solely governed by the terms of such publishing agreement and applicable law.